Metallurgical and Materials Engineering *Research paper*
Association of Metallurgical Engineers of Serbia AMES *https://doi.org/10.30544/823*

EFFECT OF FILM THICKNESS ON THE STRUCTURAL AND TRIBO-MECHANICAL PROPERTIES OF REACTIVE SPUTTERED MOLYBDENUM NITRIDE THIN FILMS

Abdelaziz Abboudi[1], Linda Aissani[2,3], Abdenour Saoudi[1], Hamid Djebaili[1]*

[1]Department of Mechanical Engineering, and Advanced Materials Laboratory (ISMA), Abbes Laghrour University, Khenchela 40000, Algeria
[2]Physics Department, Abbes Laghrour University, Khenchela 40000, Algeria
[3]Laboratory of Active Components and Materials, Larbi Ben M'Hidi University, Oum El Bouaghi, 04000, Algeria

Received 10.04.2022

Accepted 05.06.2022

Abstract

The current study aims to examine the impact of nitrogen content and film thickness on the structural and tribo-mechanical characteristics of reactive sputtered MoN thin films. Molybdenum nitride thin films with thicknesses ranging from 0.2 to 1.25 m have been applied to steel and silicon substrates for this purpose, with various amounts of controlled atmosphere ($Ar+N_2$). Then, the films are characterized using XRD (X-ray diffraction), EDX (energy dispersive X-ray analysis), SEM (scanning electron microscopy), FTIR (Fourier-transform infrared spectroscopy), and nanoindentation. The residual stress was measured using the Stoney formula. Results show that a high compressive residual stress of -5.7 GPa is present in the film with a 0.3 μm thickness and gradually decreases with increasing film thickness. Above 1 μm of film thickness, there is no change in the density of the MoN films. Also, the coating hardness and Young's modulus vary between 9.5 and 35 GPa, and 266 and 320 GPa, respectively, depending on nitrogen content and film thickness. Lastly, the friction of the MoN thin films is estimated to be around 0.55, which proves that the oxide is being slowly removed.

Keywords: reactive sputtered MoN films; atmosphere content; film thickness; FTIR spectroscopy; tribo-mechanical properties.

[*] Corresponding author: Abdenour Saoudi, *saoudi_abdenour@univ-khenchela.dz*

Introduction

Material damage due to wear or corrosion is a common problem in engineering; material resistance and functional properties are gradually reduced (e.g., mechanical, electrical, optical, aesthetic, etc.). In general, damage caused while in action can be slowed down or avoided using resistant coatings. Applying a coating to a metal substrate protects it against the corrosive agent and gives it a high surface hardness. The chosen coating must at least retain the essential functional characteristics of the substrate or even enhance them. Most thin-film applications exploit their tribological properties, mainly their low friction coefficients and high wear resistance. Their values depend on the structure, surface roughness, material composition, and environment where the friction tests are carried out. Nitrides exhibit good mechanical properties to use in various applications. They have the very high abrasion resistance and are often used as protective layers for machining tools in surface treatment. Moreover, due to their high solidity, they are also widely used for improving the mechanical properties of metal matrix composites. Otherwise, nitrides are used as the composite matrix [1]. Thin hard films are of great importance for wear-resistant, protective and decorative coatings [2]. However, the residual stress in thin films and functional coatings can intensely affect their performance. Therefore, they include thermal, growth, and intrinsic stresses generated during film deposition. Furthermore, the substrate and the overlay coating have different characteristics, such as thermal expansion coefficient, modulus of elasticity, and thickness. Therefore, residual stresses could also be generated in the film due to this difference in properties [3]. Material systems, like TiN, CrN, TaN, ZrN and MoN are intensively studied to meet modern demands [4-7].

Among them, Mo-N has attracted much attention in different applications such as catalysts, tribological, microelectronics and superconductors. Molybdenum nitrides can crystallize in different crystal structures, including γ-Mo_2N (cubic), and δ-MoN (hexagonal). γ-Mo_2N crystallizes in a FCC-structure with randomly distributed nitrogen ions in octahedral sites and has a hardness of about 33 GPa. Under high pressure, hexagonal -MoN crystallizes in a slightly distorted NiAs-type ordered structure [8, 9]. MoN is more resistant to shear deformation than γ-MoN and, hence, has the potential to achieve higher hardness. The nano–indentation test showed that -MoN thin-film coatings are 50 GPa harder than -MoN thin-film coatings [10].

Molybdenum nitride through physical vapor deposition (PVD) has many unique physical and mechanical properties, such as high hardness, low average coefficient of friction, good adhesion to steel substrates, and low residual stress [11-16]. MoN-based thin films synthesized using PVD have been reported to have excellent tribological properties at room temperature [17]. Furthermore, the MoN can be used as a protective, corrosion, and wear-resistant material due to its rigidity, chemical, thermal, and mechanical stability. Due to its electrical connection, it is used as a diffusion barrier layer in microelectronics applications [18].

For example, *N. Haberkorn et al.* made nanocrystalline MoN by crystallizing it with reactive DC sputtering at room temperature using a $N_2/(Ar+N_2)$ = 0.5 mixture. They found that the annealed MoN film had an amorphous structure and a good superconducting critical temperature at about 170 nm thickness [19].

S.M. Aouadi et al. found that the Mo_2N/MoS_2/Ag composite films show the best wear resistance with the formation of molybdenum oxide phases on wear tracks that can play a lubricating role in wear tests [20, 21]. The properties of molybdenum nitride-

based composite films attracted the interest of dural engineers. However, discussions in the tribology literature about the properties of binary MoN films in severe conditions are relatively rare.

This paper aims to examine the effects of film thickness ranging from 0.2 to 1.25 µm and nitrogen content on the structural and tribo-mechanical properties of reactive sputtered MoN thin films. The films have been analyzed and characterized for an in-depth investigation using XRD, EDX, SEM, and FTIR analyses. The FTIR technique reveals that all elements such as oxygen, carbon, hydrogen, and nitrogen play an important role during and after film deposition. The strong correlation between the characterization results, the residual stresses, and the mechanical properties confirms that the MoN film is an excellent material that can improve the tribological properties of steel.

Experiment procedure

Substrate preparation and MoN films deposition

Si (100) wafers and XC100 steel are used as substrates (see Fig. 1 a, c). We used Si (100) for the XRD analysis and to obtain the cross section of the MoN deposited films. The films deposited on the XC100 steel substrates are used to determine the mechanical and tribological performance.

Prior to the film deposition, the steel samples were mechanically polished to a mirror finish with (120-1200) using grit SiC papers, corresponding to a surface roughness Ra value of about 30 nm measured with an optical profilometer (VEECO-Wyko NT-1100). After that, the samples were ultrasonically cleaned in acetone (95°) for 10 minutes, rinsed in alcohol (95°) for 5 minutes, and dried by air before being mounted in the deposition chamber.

Molybdenum nitride coatings are performed using a reactive magnetron sputtering system through the NORDIKO 3500 PVD machine. The film deposition is carried out using substrates fixed on a sample rotating substrate-holder placed in front of the Mo target at a distance of 100 mm. The residual pressure was reduced to 6×10^{-4} Pa to minimize coating impurities and defects. Before deposition, the substrates have been ex-situ cleaned by pure trichloroethylene, acetone, ethanol, and non-ionized water. Then, the substrates and the Mo target are cleaned in situ by argon ions after reaching a vacuum pressure of 8.10^{-6} Pa. The MoN coating is then deposited on steel and silicon substrates, at floating temperature and a constant working pressure of 0.4 Pa, in an argon and nitrogen atmosphere mixture (see Fig. 1b and Fig. 1d). The purity of the used gases is: Ar (99.99 % purity), and N_2 (99.98 % purity), which are were separately injected into the chamber.

In this study, various molybdenum nitride coatings with different thicknesses ranging between 0.2 and 1.25 µm are obtained according to deposition times varying between 30 and 195 min using a deposition rate of 6.47 nm/min. Table 1 shows the essential experimental parameters of the coating deposition.

Table 1. Main parameters and chemical composition of molybdenum nitride film deposition.

Deposition condition					
N/Ar	Voltage (-V)	Power (W)	Time (min)	Thickness (μm)	$\%N_2$ in the plasma
20/80	900	350	30-195	0.2-1.25	20
Chemical composition					
N (at.%)	O (at.%)		Mo (at.%)		N/Mo ratio
42.0	2.7		55.3		0.75

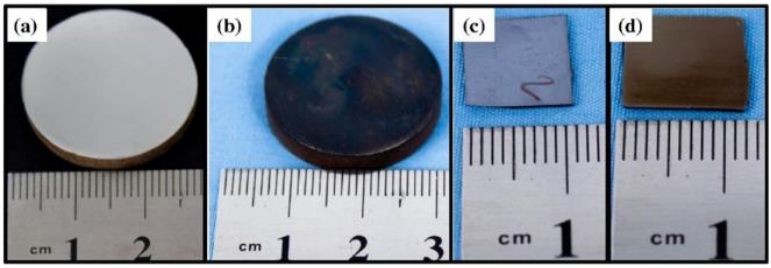

Fig. 1. a) Uncoated XC100 steel substrate, b) MoN coated XC100 steel substrates, c) Uncoated Si (100) wafer and d) MoN coated Si (100) wafer.

1.1. Characterization methods

XC100 steel substrates and Si (100) wafers are considered for analyzing the effect of film thickness on the structural properties of sputtered MoN thin films. All the samples are characterized using XRD (X-ray diffraction), EDX (energy dispersive X-ray analysis), SEM (scanning electron microscopy), and FTIR (Fourier-transform infrared spectroscopy) analysis.

IR spectra are obtained using a Perkin–Elmer spectrometer with a spectral resolution of 8 cm^{-1}. The Fourier Transform Infrared Technique (FTIR) is used in transmission mode ranging from 400 to 4000 cm^{-1}. For each sample, 120 scans are performed. After scraping, the substrate layer (around 30 mg) is ground in an agate mortar with a KBr powder (90 ±2 mg). Next, the powder is compressed in a cold 150 MPa isostatic press (CIP) to obtain a 200-250 mm thick pellet. The transmission spectra are obtained by dividing the signal transmitted through the pellet (I) by the signal measured through an aperture of the same dimensions (I_o), see equation 1. All infrared spectra show the absorbance (A) as a function of the incident wavenumbers in cm^{-1}.

$$A = -log\left(\frac{I}{I_0}\right) \qquad 1$$

The X-ray diffraction spectrum of MoN film is performed with a BRUKER D8 DISCOVER diffractometer, and all the data are collected with steps of 0.021° (2θ) by an X'Pert Highscore software. Images are then taken on a field emission scanning microscope (Jeol JSM-5900 LV 10 kV) equipped with an EDX (energy dispersive X-ray) spectroscopy system measuring the composition of the elements constituting the MoN films. Furthermore, residual stresses generated during the deposition process are measured based on the curvature method and Stoney equation [22, 23]. The curvature

rays of the samples are measured before and after coating deposition by an optical profilometer (VEECO Wyko-NT 1100). They are calculated as follows:

$$\sigma = \frac{E_s \times}{6(1-\nu_s)} \frac{t_s^2}{t_f} \left(\frac{1}{R} - \frac{1}{R_0}\right) \quad 2$$

Where σ is the residual stress, E_s is Young's modulus of the substrate, t_s is the substrate thickness, ν_s is Poisson ratio of the substrate, t_f is the film thickness, R is the coated substrate curvature radius, and R_0 is the substrate curvature radius.

The density of the layer is estimated based on the method of differential weighing compared to the coating volume. Steel substrates have been weighed before and after depositing (substrate mass m_{s0} = 17.18 ± 0.34 g). The difference between both measurements corresponds to the layer's mass.

The hardness (H) and Young's modulus (E) of thin filmsThe hardness (H) and Young's modulus (E) of thin films are measured using an MTS XP Nano-indenter equipped with a Berkovich tip. Its continuous function enables measurements with a maximum penetration depth of 150 nm. Finally, the tribological tests are carried out using a Tribometer CSM Instrument in a pion-plan configuration. The test parameters are 0.5 m/s sliding speed and a 5N normal load corresponding to the desired industrial application. Also, all the tests are carried out in dry conditions without lubrication for 10 minutes, which corresponds to a linear distance of 0.3 m. The used pin is a silicon nitride ceramic ball (Si_3N_4) with a 5 mm diameter, and the disk is driven back and forth. are measured using an MTS XP Nano-indenter equipped with a Berkovich tip. Its continuous function enables measurements with a maximum penetration depth of 150 nm. Finally, the tribological tests are carried out using a Tribometer CSM Instrument in pion-plan configuration. The test parameters are 0.5 m/s sliding speed and a 5N normal load corresponding to the desired industrial application. Also, all the tests are carried out in dry conditions without lubrication for 10 minutes, which corresponds to a linear distance of 0.3 m. The used pin is a silicon nitride ceramic ball (Si_3N_4) with a 5 mm diameter, and the disk is driven back and forth.

Results and discussions

Analysis of the MoN coating with the FTIR (Fourier-transform infrared spectroscopy) technique

The FTIR (Fourier-transform infrared) spectra reveal the composition of solids, liquids, and gases. This technique allows for the evaluation of the quality of the deposited coatings. The rapidity and ease of the FTIR (Fourier-transform infrared) analysis are particularly useful for our coatings. Also, the sensitivity of FTIR analysis makes it possible to verify the various phases existing in MoN coating. Fig.2 represents the FTIR spectra of MoN coatings deposited considering the conditions mentioned in Table 1. As indicated in Fig.2, the FTIR (Fourier-transform infrared) spectrum between 400 and 4000 cm^{-1} can be subdivided into four regions denoted I, II, III, and IV. Region (I) indicates the presence of nitrides and oxides of molybdenum (Mo-N and Mo-O). Regions (II) and (IV) are related to carbon, nitrogen, hydrogen, and oxygen contamination. Region (III) indicates the presence of N_3 and CO_2.

Importantly, the 1000-400 cm^{-1} peaks correspond to the stretching and bending vibrations of metal-oxygen and metal-nitrogen characteristic liaisons [24]. The Metal-N

stretch could shift to ~922 cm^{-1} [24]. The low-intensity peaks between 1000 and 1550 cm-1 are related to C-N, C-O, C-C, C=O, CCC, and CC=O vibrations [25]. The fine and intense peak around 1400 cm^{-1} is linked to the vibrations of the ($NH4^{+}$) groups, to which the intense peak at (~3200 cm^{-1}) is associated and corresponds to N-H [24]. The bending vibrations of O–H liaisons of adsorbed water molecules are obtained at approximately 1625 cm^{-1} [25]. The peak between 1700 and 1800 cm^{-1} is associated with the NO-Mo bond vibrations [26].

More importantly, the peak around 2450 cm^{-1} corresponds to carbon dioxide CO_2; its presence is due to the deposition technique [27]. The azide ligands ($-N_3$) create a wide absorption signal between 1900 and 2500 cm^{-1} [24]. The peaks at 2852, 2924, and 2960 cm^{-1} are linked to the CH_2 and CH_3 groups [28]. Finally, the broad peak obtained at approximately 3400 cm^{-1} is associated with OH in H_2O, associated with the peak ~ 1630 cm^{-1}.

For an in-depth analysis, our results' showed that localization of the absorption peaks is carried out using the decomposition of the lines defined by the Gaussian function peaks, see Figs. 3, 4, and 5. This method allows us to contrast the present FTIR results with those of the literature. For this purpose, three main areas in the infrared spectrum are examined. The first concerns the Mo-N and Mo-O links noticed between 400 and 1000 cm^{-1}. The second one, between 1800 and 2500 cm^{-1}, concerns the links in the azide groups, and the third one, between 3800 and 4000 cm^{-1}, concerns the N-H and O-H links.

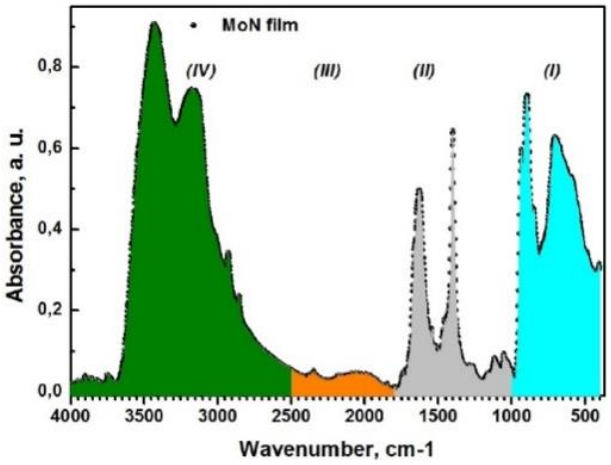

Fig. 2. FTIR (Fourier-transform infrared) spectra of the MoN films in the 400-4000 cm^{-1} spectral range.

Fig. 3 represents the FTIR (Fourier-transform infrared) spectra of the molybdenum nitride films in the 400-1000 cm^{-1} range. The curves are decomposed into Gaussian function peaks. The existence of oxygen in the MoN films can produce peaks corresponding to the molybdenum oxide and C-O and O-C=O species. The oxygen impurity that is detected in the MoN films is due to the residual oxygen in the vacuum chamber and the affinity of Mo for oxygen during deposition or post-deposition films.

From the FTIR fits, we can estimate the nominal composition of Mo-N and Mo-O at the surface of the MoN film. The lines correspond mainly to the vibration bending

and then stretching of the Mo-O and Mo-N bands. *Melissa E. Kreider et al.* [29] indicated that the passivation layer of the Mon films is due to the existence of oxygen and produces the oxide phase.

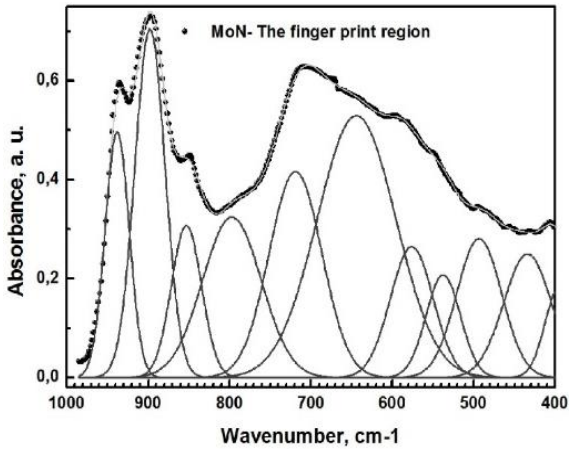

Fig. 3. FTIR (Fourier-transform infrared) spectra of the MoN films in the 400-1000 cm^{-1} fingerprint region.

Fig. 4 represents the FTIR (Fourier-transform infrared) signatures in the 1800-2500 cm^{-1} range, which generally correspond to the signal of azide groups. These FTIR curves are smoothed and decomposed into constituent peaks. According to the reference [24], the values between 2083-2094 cm^{-1} correspond to the vibrations of ν (C-N). The 1944 cm^{-1} value corresponds to the vibration of ν (C-O). Other investigations attribute the 2034 cm^{-1} and 2056 cm^{-1} values to the ν as -N_3 vibrations, and the 2236 cm^{-1} value corresponds to ν as NCO [30]. According to *A. Chithambararaj et al.* [24], the bands at 2033 and 2151 cm^{-1} are linked to the azide bound and cyanide group (C≡N), respectively. An additional mode at 2048 cm^{-1} belongs to free azide, while at 2092 cm^{-1} belongs to free HCN [31]. The bands at 2300-2400 cm^{-1} are also attributed to the stretching of the C=N bond [32]. The bands at 2362 cm^{-1} and 2340 cm^{-1} correspond to the CO_2 [27].

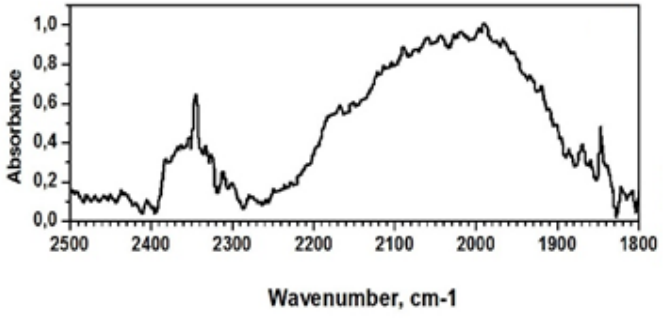

Fig. 4. FTIR (Fourier-transform infrared) spectra of the MoN film in the 1800-2500 cm^{-1} spectral range.

Fig. 5 represents the 2400-3800 cm^{-1} range of the molybdenum nitride spectrum. This proportion of the spectrum usually contains information about CH_2/CH_3 groups, N-H liaisons, and O-H liaisons in H_2O, respectively. As shown, the part relating to the N-H signature [33] is more pronounced and very clear in the MoN coating.

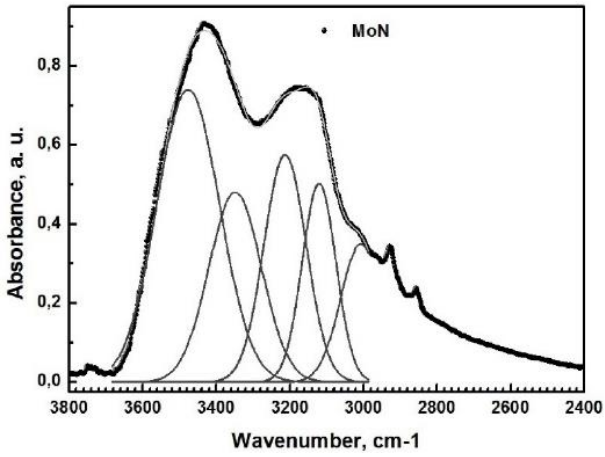

Fig. 5. FTIR spectrum of the MoN film in the 2400-3800 cm^{-1} spectral range.

XRD (X-ray diffraction) analysis, SEM (scanning electron microscopy) observations, and EDX (energy dispersive X-ray) composition elements

The X-ray diffraction spectrum of MoN film is shown in Fig. 6. An extended peak, poorly defined around 69°, represents the silicon substrate on which the film has been deposited. The JCPDS files showed a weak signal for MoN, for which the most intense peaks are located (between 35 and 40°).

However, due to the thinness of the film, no preferential orientations for the Mo-N phases were observed in the X-ray diffraction spectrum, as previously confirmed [19]. Additionally, subjected to molybdenum oxides, for which the maximum intensities are around 20 to 30°, the signal is also weak. We believe that this analysis shows that the quantity analysed is relatively low and that the amorphous character of the layer probably does not allow for obtaining convincing crystalline peaks.

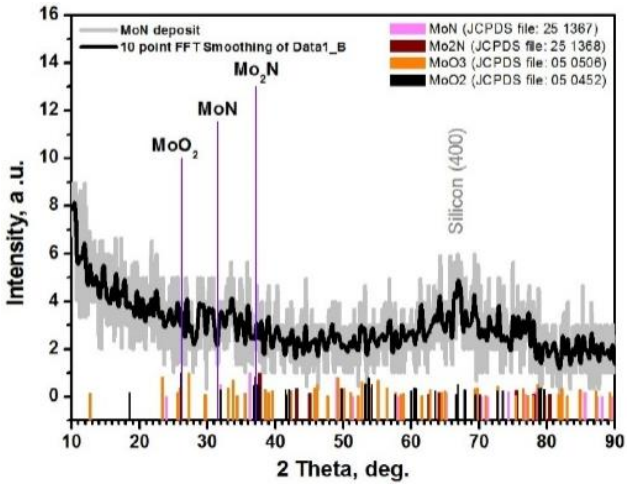

Fig. 6. X-ray diffraction spectrum of MoN film.

The SEM (scanning electron microscopy) images of the coatings (sectional view and front view) are shown in Figs. 7a and 7b. The sectional view of the MoN coatings showed a columnar structure with an increase in the film thickness of 1.1 and 1.25 µm with increasing the deposited time from 150 to 120 min, respectively. The front view shows that the coating exhibited a relatively homogeneous surface with the presence of white spots for the MoN coating, with a small thickness indicating a rough surface (Fig. 7d). The EDX analyses presented in Figs. 7 c, and f confirmed the presence of Mo, N, and O elements, which would confirm the molybdenum nitride phase. The presence of oxygen tends to reinforce the presence of other phases, such as molybdenum oxynitride.

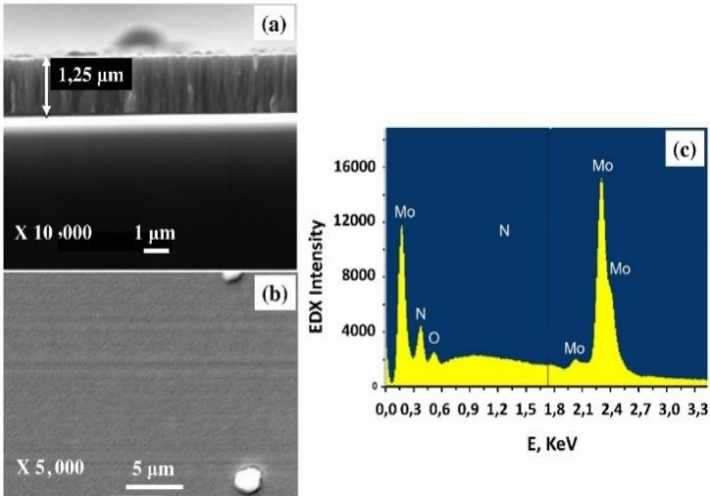

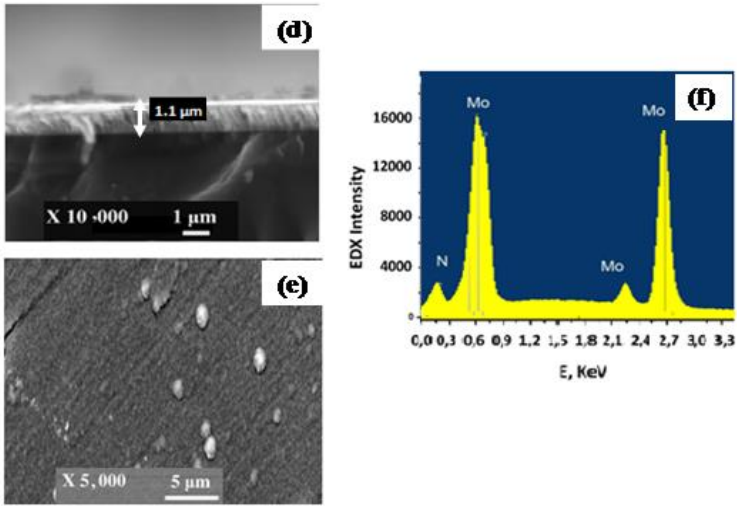

Fig. 7. SEM images of the MoN films: a, d) sectional view b, e), surface view of the coating, and c, f) EDX spectrum of MoN film deposited at 150 to 120 min.

Effect of film thickness on residual stresses and density

Residual stresses can be determined experimentally by various techniques: X-ray diffraction (the sin 2ψ method) [3], Synchrotron ray diffraction, Neutron ray diffraction, Ultrasonic method, Curvature method [22-23, 34, 35], Incremental hole method, EBSD (Electron Back Scattered Diffraction) techniques. Fig. 8 shows the variations in the internal stress and the density of the deposited MoN film through its thickness. The high obtained values of compressive stresses are justified by the effects of growth and thermal stresses. Other studies have reported a similar value of -4 GPa for the presence of interstitial nitrogen [36]. The residual stress of the MoN coating was determined by using the Stoney formula [22-23]. As reported in the literature, MoN film presents compressive stress. The maximum stress of – 4.6 GPa is obtained in the MoN thin film of 0.2 µm thick. The compressive state of the residual stress is beneficial for a coated structure and enhances its life duration. This prevents cracks and other defects that cause deterioration. The compressive stresses ameliorate the film resistance to fatigue and certain forms of corrosion stress. The molybdenum nitride coating is a passivating layer and protects against further surface oxidation. The introduction of high compressive stresses could achieve the amelioration of fatigue life.

Hones and Rickerby models [37-39] provide further explanations relating to the aspects and thicknesses of deposited layers. Rickerby's model shows dense columnar growth where the increase in layer thickness is associated with the increase in column diameters. Increasing the coating thickness led to a decrease in the film stress. Importantly, there is no longer a significant change at 1 µm film thickness. The layers then appeared in an equilibrium state, which indicated that ion bombardment had become negligible with the columnar growth of the layers governed by shading effects, as shown in the Hones model relating the growth of the columns to constraint reduction.

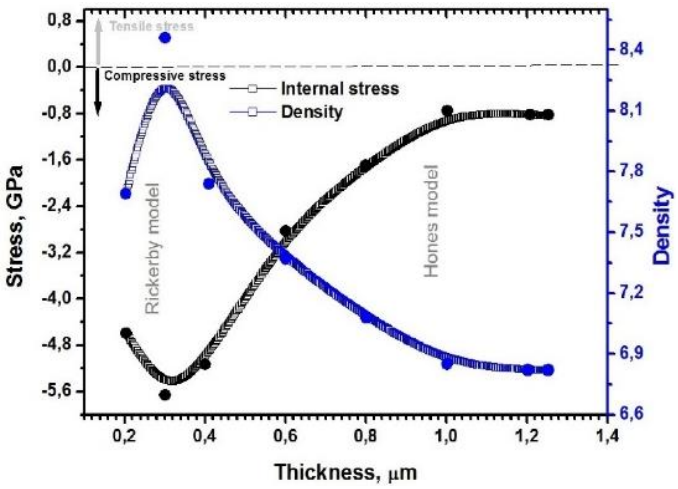

Fig. 8. Variation of the internal stress and density as a function of MoN film thickness.

Some authors [40] adopted a model combining Rickerby's and Hones' models relating the growth of columns to stress reduction. The basic principle is doing a coating deposition with a homogenous and dense structure. It has been found lower for our MoN film, which means that coating contains porosities and other less dense phases. These existents in the molybdenum-based alloys would be the oxides exhibiting a low density of about 4.6 and the molybdenum carbide of 8.9 density. The density of our MoN coating is estimated between 6.8 and 8.5 depending on the thickness of the deposited coatings, Fig. 8. A lower density at the surface means that the outer layer is rich in oxygen, which decreases it and reinforces the presence of the Molybdenum oxynitride phase. Indeed, a thicker layer would contain a higher quantity of porosities, which tends to decrease its density.

According to Hones and Ricker by models [37-39], the maximum film density coincides with the highest stress. The lowest density corresponds to the lowest stress and the highest thickness, see Fig. 8.

Variation of the hardness and young modulus as a function of MoN film thickness

Fig. 9 presents the hardness and young modulus of MoN film versus the film thickness. The hardness of the coatings is between 9.5 and 35 GPa. According to *A. Gilewicz et al.* [41], the MoN coatings' hardness depends on the phase composition (23-24 GPa). Earlier studies reported that the hardest MoN films were mainly attributed to the high compressive residual stress and the fine grain [10].

We find that these two parameters (hardness and Young's modulus) decrease with increasing deposit thickness. The decrease in hardness is probably also explained by the film densification and surface roughness. This behavior can be attributed to an increase in the density of point defects; this effect has been shown previously by the appearance of more spots in film surface.

Hardness is often the primary criterion defining the wear resistance, but Young's modulus is also essential. According to Leyland et al. [42], the high H/E is an excellent criterion of durability for a coating used in mechanical applications under heavy loads. These ratios characterize the elastic behavior of the material and the load necessary to

initiate plastic deformation [42]. For our films, Young's modulus varies between 266 and 320 GPa, depending on the film thickness.

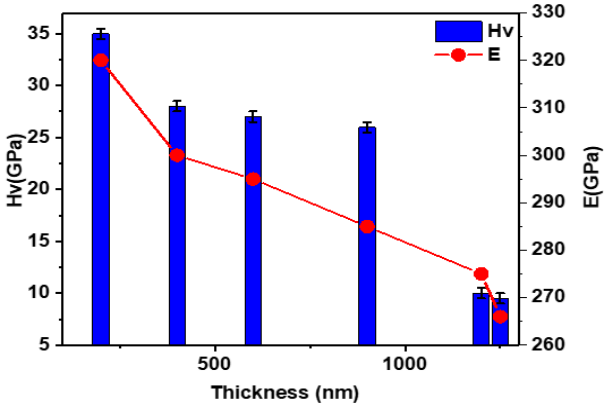

Fig. 9. Hardness and Young's modulus in the MoN film vs thickness.

Variation of friction coefficient as a function of MoN film thickness

Fig. 10 presents the evolution of the friction coefficient of the MoN coatings depending on the film thickness. We notice that the friction coefficient of the MoN film tested against a Si_3N_4 ball is between 0.55 and 0.93. The COF is close to that obtained for the sputtered MoN films [43].

Moreover, with increasing the film thickness, the coefficient of friction gradually decreased. This decrease is also caused by the contamination of the Mo-N films by oxygen and the subsequent formation of oxides. These oxides act as a lubricating medium between the layer and the substrate. However, this value is due to the gradual elimination of oxides and the surface's homogeneity. These results are in good agreement with those of other recent studies [43-45].

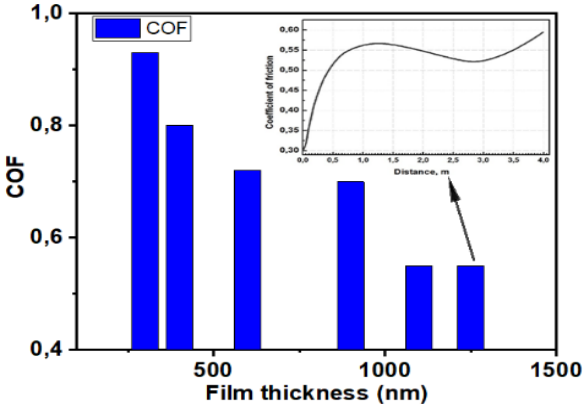

Fig. 10. Evolution of the friction coefficient of the MoN film vs sliding distance.

Conclusion

Molybdenum nitride (MoN) thin films with thicknesses ranging from 0.2 to 1.25 m were deposited on silicon and steel substrates using the reactive magnetron sputtering technique in various controlled atmosphere ($Ar+N_2$) contents. The findings reported in this study are summarized below.

FTIR spectroscopic analyses presented the existence of four regions: between 400 and 1000 cm^{-1}, the first part showed Mo-N and MoO liaisons. Between 1000 and 1650 cm^{-1}, the second part showed the various liaisons of C, O, N, and H elements. Between 1800 and 2500 cm^{-1}, the third part showed the azide groups, the $M-N_3$ liaisons, and CO_2 in the medium during the deposition. The fourth part, for the region between 2800 and 4000 cm^{-1} gave information on the CH_n, H-N, and OH groups.

Moreover, the tribo-mechanical properties of these thin films have been evaluated to determine their performance. It is found that the residual stresses generated during the deposition process are compressive and range between -5.6 and -0.75 GPa, depending on the film thickness. The densities of our MoN coating are estimated at 6.8 and 8.5 depending on the thickness of the deposited coatings. The lower density at the surface means that the outer layer is rich in oxygen, which decreases its brittleness and reinforces the presence of the molybdenum oxide phase. Indeed, the thicker layer would contain a higher quantity of porosities, which tends to decrease its density. The MoN coating hardness and Young's modulus vary between 7.5 and 35 GPa, 266 and 320 GPa, respectively, depending on nitrogen percentage. Due to the gradual oxide elimination and the surface homogeneity, MoN thin-film presents a lower friction coefficient of about 0.55 at 1.25 μm of film thickness.

References

[1] W. Lengauer: Encyclopedia of Inorganic Chemistry, 2005 John Wiley & Sons, Ltd, (2015) 1-24.

[2] F. Lévy, P. Hones, P. E. Schmid, R. Sanjinés, M. Diserens, C. Wiemer: Surface and Coatings Technology, 120 (1999) 284-290.

[3] C. Sarioglu, U. Demirler, M. K. Kazmanli, M. Urgen: Surface and Coatings Technology, 190 (2005) 238-243.

[4] K. H. Kim, E. Y. Choi, S. G. Hong, B. G. Park, J. H. Yoon, J. H. Yong: Surface and Coatings Technology, 201 (2006) 4068-4072.

[5] J. E. Sundgren: Thin Solid Films, 128 (1985) 21-44.

[6] S. C. Lee, W. Y. Ho, F. D. Lai: Materials Chemistry and Physics, 43 (1996) 266-273.

[7] K. Y. Liu, J. W. Lee, F. B. Wu: Surface and Coatings Technology, 259(2014) 123-128.

[8] H.Luo, G. Zou, H. Wang, J. H. Lee, Y. Lin, H. Peng, Q. Lin, S. Deng,E. Bauer, T. M. McCleskey,A. K. Burrell, Q. Jia:The Journal of Physical Chemistry C, 115 (2011) 17880-17883.

[9] Y. Zhang, N.Haberkorn, F.Ronning, H. Wang, N. A. Mara, M.Zhuo, L. Chen, J. H. Lee, K. J. Blackmore, E. Bauer, A. K. Burrell, T. M. McCleskey, M. E. Hawley, R. K. Schulze, L.Civale, T. Tajima,Q. Jia:Journal of the

[10] S.Wang , D. Antonio , X. Yu, J. Zhang, A. L. Cornelius, D. He, Y. Zhao: Scientific Reports, 5 (2015) 13733.

[11] G. Gassner, P. H. Mayrhofer, K. Kutschej, C. Mitterer, M. Kathrein: Surface and Coatings Technology, 201 (2006) 3335-3341.

[12] G. Zhang, T. Fan, T. Wang, H. Chen: Applied Surface Science, 274 (2013) 231-236.
[13] A. Ozturk, K. V. Ezirmil, K. Kazmanli, M. Urgen, O. L. Eryilmaz, A. Erdemir: Tribology International, 41 (2008) 49-59.
[14] N. Solak, F. Ustel, M. Urgen, S. Aydin, A. F. Cakir: Surface and Coatings Technology, 174 (2003) 713-719.
[15] M. K. Kazmanli, M. Ürgen, A. F. Cakir: Surface and Coatings Technology, 167 (2003) 77-82.
[16] T. Suszko, W. Gulbinski, J. Jagielski: Surface and Coatings Technology, 200 (2006) 6288-6292.
[17] H. Kindlund, D. G. Sangiovanni, I. Petrov, J. E. Greene, L. Hultman: Thin Solid Films, 688 (2019) 137479.
[18] J. Musil, Š. Kos, S. Zenkin, Z. Čiperová, D. Javdošňák, R. Čerstvý: Surface and Coatings Technology, 337 (2018) 75-81.
[19] N. Haberkorn, S. Bengio, H. Troiani, S. Suárez, P. D. Pérez, M. Sirena, J.Guimpel: Thin Solid Films, 660 (2018) 242-246.
[20] S. M. Aouadi, Y. Paudel, B. Luster, S. Stadler, P. Kohli, C. Muratore, C. Hager, A. A. Voevodin: Tribology Letters, 29 (2008) 95-103.
[21] S. M. Aouadi, Y. Paudel, W. J. Simonson, Q. Ge, P. Kohli, C. Muratore, A. A. Voevodin: Surface and Coatings Technology, 203 (2009) 1304-1309.
[22] G. G. Stoney: Proc. R. Soc. Lond. 82 (1997).
[23] A. Mézin: Surface and Coatings Technology, 200 (2006) 5259-5267.
[24] A. Chithambararaj, A. C. Bose: Journal of Alloys and Compounds, 509 (2011) 8105-8110.
[25] I. M. McIntosh, A. R. L. Nichols, K. Tani, E. W. Llewellin: American Mineralogist, 102 (2017) 1677-1689.
[26] S. Yang, Y. Li, J. Xu, C. Li, Q. Xin, I. R. Ramos, A. G. Ruiz: Physical Chemistry Chemical Physics, 2 (2000) 3313-3317.
[27] Z. Zhang, X. Li: Procedia Environmental Sciences, 18 (2013) 353-358.
[28] N. Jasin, M. G. Tay, H. F. Hashim: Malaysian Journal of Analytical Sciences, 21 (2017) 1195-1202.
[29] M. A. Py, K. Maschke: Physica B+C, 105 (1981) 370-374.
[30] V. Sargentelli, A.V. Benedetti, A. E. Mauro: Journal of the Brazilian Chemical Society, 8 (1997) 271-274.
[31] D. Parul, G. Palmer, M. Fabian: The Journal of Biological Chemistry (JBC), 285 (2010) 4536-4543.
[32] S. N. Timmiati, A. A. Jalil, S. Triwahyono, H. D. Setiabudi, N. H. R. Annuar: Applied Catalysis A: General, 459 (2013) 8-16.
[33] L. A. D. Alejo, E. C. M. Campos, J. U. Chavarín, R. S. Fonseca, M. A. G. Sánchez: International Journal of Polymer Science, (2013) 323854.
[34] L. Aissani, A. Alhussein, C. Nouveau, L. Radjehi, I. Lakdhar, E. Zgheib: Surface and Coatings Technology, 374 (2019) 531-540.
[35] L. Aissani, A. Alhussein, A. Ayad, C. Nouveau, E. Zgheib, A. Belgroune, M. Zaabat, R. Barille:Thin Solid Films, 724 (2021) 138598.
[36] L. Stober, J. P. Konrath, V. Haberl, F. Patocka, M. Schneider, U. Schmid: Journal of Vacuum Science & Technology A, 34 (2016) 021513.
[37] S. J. Bull, D. S. Rickerby: Surface and Coatings Technology, 43 (1990) 732-744.
[38] P. Hones, R. Sanjinės, F. Lėvy: Thin Solid Films, 332 (1998) 240-246.

[39] B. W. Karr, I. Petrov, P. Desjardins, D. G. Cahill, J. E. Greene: Surface and Coatings Technology, 94 (1997) 403-408.
[40] L. Chekour, C. Nouveau, A. Chala, C. Labidib, N. Rouagd, M. A. Djouadi: Surface and Coatings Technology, 200 (2005) 241-244.
[41] A. Gilewicz, B. Warcholinski, D. Murzynski: Surface and Coatings Technology, 236 (2013) 149-158.
[42] A. Leyland, A. Matthews: Wear, 246 (2000) 1-11.
[43] C. Liu, H. Ju, L. Yu, J. Xu, Y. Geng, W. He, J. Jiao: Coatings, 9 (2019) 734.
[44] H. Ju, R. Wang, W. Wang, H. Luo, L. Yu, H. Luo: Surface and Coatings Technology, 401 (2020) 126238.
[45] J. Qian, S. Li, J. Pu, Z. Cai, H. Wang, Q. Cai, P. Ju: Surface and Coatings Technology, 374 (2019) 725-735.